Liquid springs for high-speed contamination-free manipulation of droplets and solid particles

Haibo Zhao[1,2], Hewei Du[2], Qiyu Deng[1], Wei Li[1], Mingliang Guo[2], Yiyuan Zhang[4], Liqiu Wang[4]*, Peng Yu[2,3,5]*

1) Department of Mechanical Engineering, The University of Hong Kong, Hong Kong, China

2) Department of Mechanics and Aerospace Engineering, Southern University of Science and Technology, Shenzhen, 518055, China

3) Guangdong Provincial Key Laboratory of Turbulence Research and Applications, Southern University of Science and Technology, Shenzhen,518055, China

4) Department of Mechanical Engineering, The Hong Kong Polytechnic University, Hong Kong, China

5) Center for Complex Flows and Soft Matter Research, Southern University of Science and Technology, Shenzhen, 518055, China

Accurate and flexible control of droplets is essential in many industrial applications, such as water harvesting, chemical assays, and biological detection. Magnetic force-based methods have been broadly exploited to fulfill the goals due to the advantage of non-contact, easy control, and long-range navigation. Nevertheless, it still suffers from some challenges, such as sample fouling, and the paradox between the droplet efficient motion and the large volume. Here we propose a ferrofluid-based liquid spring to achieve contamination-free and fast droplet transportation on non-wetting solid surfaces. The liquid spring is based on the actuation of a ferrofluid droplet in an external uniform magnetic field. The actuation enables the liquid spring to propel tiny objects, including the non-magnetic miscible droplets and water-repellent solid particles, with adjustable motion velocity. Furthermore, the magnetic force, applied on the ferrofluid via an additional permanent magnet, makes it possible to navigate the liquid spring in a programmable way. With the aid of the liquid spring, the single or multiple droplets/solid particles advancing, on-demand droplets coalescence, and out-of-plane droplet motion are achievable.

Introduction

Navigating tiny liquid droplets is prevalent and critical in various realms, such as Nepenthes alata[1], Namib Desert beetle[2], and cactus[3] in nature, which collect water for living, or microfluidics[4,5], bioanalysis[6,7], and heat transfer[8,9] in industry where the droplet functions as agents or vessel. Nature inspiration and industry demand motivate researchers to keep pursuing more and more flexible and accurate methods to regulate droplet motion. Generally speaking, the ways to navigate the droplet motion can be classified into two categories: passive and active control. The passive control involves the structure construction or anisotropic chemical modifications of the substrate, such as the micro-pillar[10,11] or slippery liquid-impregnated (SLIP)[12,13]surfaces. Due to the preset directions or routes, passive control generally lacks flexibility and is limited to short and inefficient liquid transportation[14]. To overcome such inadequacies, researchers have applied external stimuli for active control, such as electricity[15–17], magnetic force[18–22], light[23–25], thermal energy[26–28], acoustic force[29,30], and mechanics[31–33], to maneuver liquid droplets and fulfill more complicated tasks. Among them, the magnetic stimulus has the advantage of non-contact, easy control, and long-range transportation. Various strategies have been prepared to employ the magnetic force to manipulate the droplet motion. For example, the magnetic-responsive array-structured surfaces[34,35], magnetic additives inside the sample droplets[36], and the magnetic control

steel-beads[37]. Albeit exploited broadly, the magnetic methods still suffer from several drawbacks, such as the biofouling resulting from mixing the magnetic particles with the samples or the limited transportation speed due to the retard response of the magnetic structures.

Here, we report a liquid spring, which is able to achieve fast and contamination-free droplet transportation on non-wetting solid surfaces. The liquid spring is based on the actuation of a ferrofluid droplet in an external uniform magnetic field. When a ferrofluid droplet is placed in an external uniform magnetic field and the magnetic field is turned on instantaneously, the droplet undergoes a fascinating behavior known as stretching and retraction. This behavior repeats many times due to the competition between the magnetic, surface tension, inertial, and viscosity forces. The oscillation makes the ferrofluid droplet behave as a liquid spring, which can flick away the tiny objects with adjustable velocity, including the non-magnetic miscible droplets and water-repellent solid particles. Compared with other magnetic strategies to actuate droplets, the ferrofluid droplet-based liquid spring has three distinct merits: 1) reconciling the efficient transportation and large droplet volume. Specifically, the liquid spring can navigate the target droplet (≈ 20 μL) with high motion velocity ($\approx 19\ \mathrm{cm\ s^{-1}}$), which is fourfold higher than other reported magnetic strategies[36,38,39]. In addition, the motion velocity has a proportional correlation with the instant variation value of magnetic field strength, which can be accurately and on-time tuned by the electric current due to the usage of the Helmholtz coil. 2) contamination-free transportation. In the successful propulsion of the non-magnetic miscible droplets, the air cushion will persist between the liquid spring and the target droplet throughout the collision process. Hence there is no ferrofluid residual remaining on the target, which achieves contamination-free droplet transportation. 3) programmable motion. Due to the magnetic responsive characteristic, it is capable of leveraging a permanent magnet to achieve programmable and on-demand motion of the liquid spring, initiating its propulsion process from any designed location on the substrate. Additionally, the liquid spring can be adopted to propel non-magnetic water-repellent solid particles and solid-liquid-solid object sequence, which is rarely reported in other magnetic strategies[40]. Thus, our work provides a facile and flexible strategy for manipulating tiny objects in efficient and programmable ways, which shows great potential in various applications, including biomedical assays and material sieving.

The liquid spring

The working mechanism of the liquid spring is based on the actuation of a ferrofluid droplet within an external uniform magnetic field (Fig. 1a). Ferrofluid is an intelligent material composed of ferromagnetic nanoparticles, carrier liquid, and surfactant[41]. The ferromagnetic nanoparticles in the carrier liquid make the ferrofluid responsive to a magnetic field, enabling the flexible and reversible control of a ferrofluid droplet. When a ferrofluid droplet is laid within an external uniform magnetic field, the permeabilities variance between the ferrofluid and its surrounding medium redistributes the magnetic field[42–45], causing a non-uniform magnetic field near the ferrofluid droplet (Fig. 1b, Video V3, Supporting Information). The gradient of the magnetic field $\boldsymbol{H}$ incurs the magnetic force, which elongates the ferrofluid droplet. Fig. 1b illustrates the numerical distribution of the magnetic field strength H in the elongation process. H at the top and bottom ends of the droplet exceeds that at the left and right ends, which is quantitatively verified by the distribution of H along the vertical and horizontal axes of the droplet (Fig. 1c). This indicates that the droplet experiences a stronger magnetic force F_{m} at the top and bottom ends because in the linear ferrofluid, the magnetic force is proportional to H^2 (Supporting Information Section 2). It explains

the vertical elongation of the droplet. Furthermore, due to the axisymmetric distribution of H, no net force is applied on the ferrofluid droplet. As a result, the droplet solely undergoes morphological transformations without experiencing any displacement of its centroid.

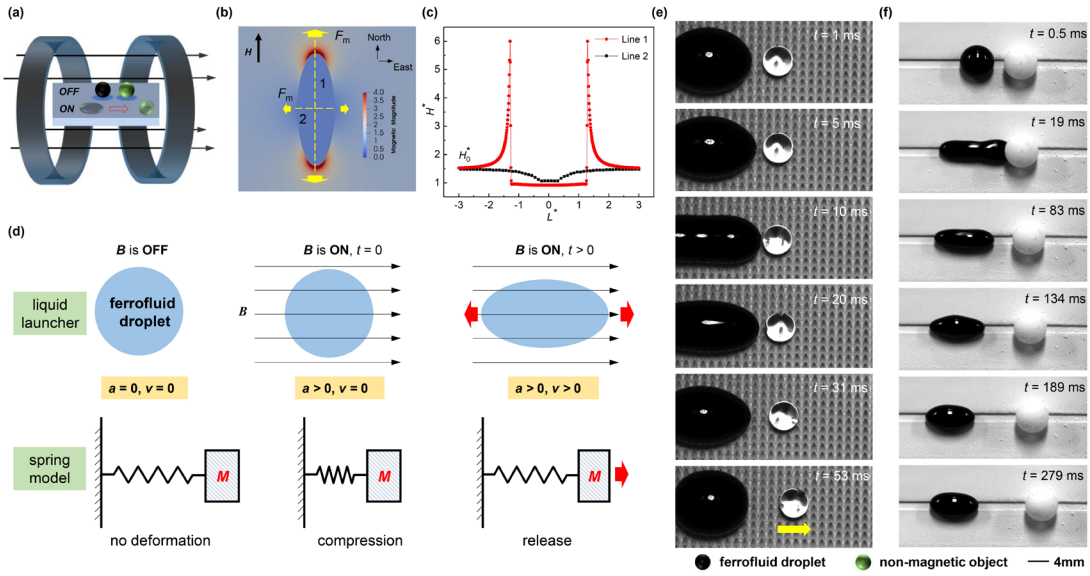

Fig. 1 The mechanism and usage of a liquid spring. (a) A ferrofluid droplet (black color) is elongated in an external uniform magnetic field and propels a non-magnetic object (green color). **(b)** The numerical demonstration of the magnetic force acting on the ferrofluid droplet induced by the non-uniform magnetic field around the droplet. The ferrofluid droplet is elongated along the magnetic field direction due to the stronger magnetic force at the top and bottom ends of the droplet. The net magnetic force equals zero so that the droplet mass centroid keeps stationary in the elongation process. **(c)** The numerical distribution of the magnetic field strength along Lines 1 and 2 delineated in **(b)**. **(d)** The metal spring model for describing the ferrofluid droplet deformation in an external uniform magnetic field. When the magnetic field is deactivated, the droplet is as relaxed as the metal spring without deformation. The acceleration (***a***) and the velocity (***v***) of droplet tips both equal zero. When the magnetic field is activated, it will fuel the ferrofluid droplet with magnetic energy as a metal spring is filled with the elastic potential energy after compression. The acceleration is larger than zero and the velocity still equals zero. Afterward, the ferrofluid droplet is elongated, which resembles the release of a compressed metal spring. The acceleration and the velocity are both larger than zero. When the magnetic field is deactivated, the droplet retracts to its original shape and the process is reversible. **(e)** The liquid spring flicks away a non-magnetic miscible droplet on a superhydrophobic surface when the magnetic field is activated. **(f)** A ferrofluid droplet propels a water-repellent solid particle when the magnetic field is activated.

The deformation process of a ferrofluid droplet subject to an external uniform magnetic field resembles the compression and release of a metal spring by mechanical force (Fig. 1d). Initially, the instantaneous activation of the magnetic field infuses the ferrofluid droplet with magnetic energy, akin to the accumulation of elastic potential energy in a compressed metal spring. The magnetic energy is relevant to the instant variation value of the magnetic field strength. Subsequently, the droplet undergoes rapid stretching, resembling the release of a compressed spring. After deactivating the magnetic field, the droplet retracts back to its original shape. In the present work, the magnetic field is generated by the Helmholtz coil and the field strength is directly proportional to the electric current, which makes the control of the stretching-retraction process accurate and reversible. In this way, a ferrofluid droplet subject to an external uniform magnetic field can be regarded as a liquid spring. The 'elasticity' of the liquid spring is related with the stretching velocity and is able to be adjusted by varying the instant variation value of the magnetic field strength. This characteristic enables the liquid spring to propel small objects, e.g., the non-magnetic miscible

droplets and water-repellent solid particles, with desired velocities. For example, when an aqueous droplet is placed adjacent to a water-based liquid spring on a superhydrophobic surface and they are aligned with the magnetic field direction, the liquid spring will stretch and move closer to the aqueous droplet upon the activation of the magnetic field (Fig. 1e). If the size of the liquid spring is significantly larger than that of the target droplet, an air cushion between the liquid spring and the target droplet forms and persists in the collision process, preventing their coalescence. As a result, the aqueous droplet is propelled away due to the transferred momentum and the extremely low friction on the surface. For the successful propulsion of a miscible droplet using the liquid spring, it is essential that the air cushion has to persist throughout the entire collision process. Otherwise, the coalescence of the liquid spring and the target droplet will occur. The propulsion of a non-magnetic superhydrophobic solid particle is easily achievable owing to its intrinsic water-repellent characteristic (Fig. 1f).

Dynamics of a ferrofluid droplet undergoing the induced magnetic density instant variation

The dynamics of a ferrofluid droplet within an external uniform magnetic field, which is the essence of the liquid spring actuation, is explored in this section. A ferrofluid droplet with the initial diameter L_0, deposited on the superhydrophobic solid surface within an external uniform magnetic field, will undergo morphology oscillations when the magnetic field is activated or deactivated instantaneously (Fig. 2a). It is figured out that the maximum deformation in each oscillation gradually diminishes, which is attributed to two primary factors: the viscous dissipation of the droplet itself and the friction between the droplet and the solid substrate. Eventually, the ferrofluid droplet achieves the equilibrium deformation L_f, which is determined by the competition between the magnetic force and the surface tension. Fig. 2b illustrates the impact of the droplet volume Ω and the induced magnetic density magnitude B on the dimensionless equilibrium length of the droplet $\widetilde{L_\mathrm{f}}$, defined as the ratio of L_f to L_0. It is figured out that both B and Ω have the influences on $\widetilde{L_\mathrm{f}}$. Indeed, a larger Ω corresponds to a stronger stretching force, as the magnetic force acts on the body of the ferrofluid droplet. The intensified stretching force heavily deforms the ferrofluid droplet. The 'elasticity' of the liquid spring is related with its maximum deformation rate λ in the oscillations, generally observed during the initial oscillation. λ in the oscillation dynamics is dependent on the instant variation value of the induced magnetic density ΔB and Ω (Fig. 2c). When the ferrofluid droplet is small, the magnetic force is not sufficiently strong to overcome the surface tension and viscous forces. As a result, it takes a longer time for the droplet to deform from its initial profile to the maximum profile. However, as Ω increases, the magnetic force becomes more pronounced, exceeding the effect of viscous forces and the incremental surface tension. Consequently, λ increases with Ω.

During the process of ferrofluid droplet stretching, the central region experiences thinning due to the flow motion from the middle toward the ends. When ΔB is small, the droplet acquires a relatively low amount of magnetic energy in the stretching process, resulting in a kinetic energy that is smaller than the surface energy. As a result, the thinnest part of the droplet remains intact throughout the stretching process (Video V4, Supporting Information). However, as ΔB intensifies or Ω expands, the flow velocity towards both ends increases significantly due to a larger magnetic energy. The inertial effects may outweigh the surface tension. Consequently, the thinnest part of the ferrofluid droplet undergoes breakup, resulting in the formation of two main daughter droplets and a smaller satellite droplet derived from the filament in the middle region (Fig. 2d, Video V5,

Supporting Information). The ultimate results are dependent on Ω and ΔB as both factors can alter the magnetic force exerted on the droplet interface. Fig. 2e depicts two distinct regimes governing the outcome of the stretching process in terms of the dimensionless volume $\tilde{\Omega}$ ($=\Omega/\Omega_0$, where Ω_0 is the droplet volume with radius $= 1$mm) and the magnetic bond number $\mathrm{Bo_m}$ ($=(\Delta B)^2 L_0/(\sigma_0\gamma)$, where σ_0 and γ are the vacuum permeability and the surface tension coefficient). As $\tilde{\Omega}$ increases, the magnetic effect becomes increasingly prominent and smaller $\mathrm{Bo_m}$ is able to break up the ferrofluid droplet. During the propulsion process, the impact force that a ferrofluid droplet imposes on the target is related with its motion velocity. The target effectively utilizes the transferred momentum to overcome the initial pinning force and subsequent friction encountered throughout the motion process. Fig. 2f illustrates the impact force values F_i, measured using a cantilever force sensor for an 80 μl ferrofluid droplet. As ΔB increases, the impact force is intensified for moderate ΔB. However, when the resilient force, acting on the ferrofluid droplet by cantilever, is larger than the droplet pinning force and friction, the ferrofluid droplet centroid will not keep stationary in the impacting process and it moves along the resilient force direction. Thus, the deformation of the cantilever is attenuated, which results in the mild changes of F_i for larger ΔB.

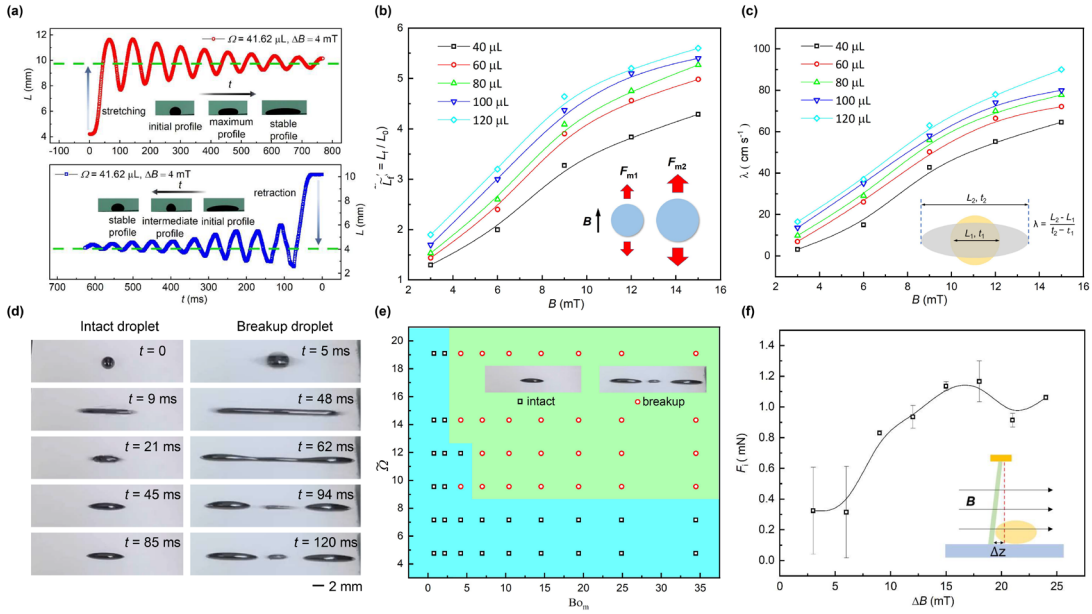

Fig. 2 The dynamical response of a ferrofluid droplet experiencing an induced magnetic density instant variation. (a) The two panels show the temporal evolution of the ferrofluid droplet profile when the magnetic field is activated (top) or deactivated (bottom) instantaneously. The ferrofluid droplet experiences oscillation due to the competition between the magnetic force, inertial force, viscous force, and surface tension. The maximum deformation declines in each oscillation and eventually the ferrofluid droplet reaches an equilibrium state. **(b)** Dependence of the dimensionless droplet stable profile $\tilde{L}_\mathrm{f}$ on the volume Ω and the induced magnetic density magnitude B. The competition between the magnetic force and the surface tension determines the final droplet profile. A stronger magnetic field induces a longer droplet profile. A larger ferrofluid droplet, bearing a stronger magnetic force, deforms heavily. **(c)** Correlation of the ferrofluid droplet maximum deformation rate λ with the instant variation value of the induced magnetic density ΔB for different droplet volume Ω. λ can reach up to 89.4 $\mathrm{cm\,s^{-1}}$. **(d)** Two typical scenarios of the ferrofluid droplet deformation dynamics for different Ω. The first scenario is that the droplet keeps intact throughout the dynamics (left panel, $\Omega = 40$ μl, $\Delta B = 10$ mT). The reason is that the inertial effect is not comparable with the surface tension and the droplet keeps intact afterward. The second one is that the inertial effect outweighs the surface tension so that the droplet is divided into two main daughter droplets and a satellite droplet in the stretching process (right panel, $\Omega = 60$ μl, $\Delta B = 10$ mT). **(e)** The two distinct regimes for the outcome of the droplet deformation under different $\tilde{\Omega}$ and $\mathrm{Bo_m}$ are illustrated. **(f)** Dependence of the impact force on ΔB. The impact force is on the order of millinewton, which is comparable with the droplet gravity ($\Omega = 80$ μl).

Utilizing the water-based liquid springs to manipulate the aqueous droplets

With the elasticity, the liquid spring can be utilized to propel the miscible droplets. Fig. 3 illustrates the typical strategies to manipulate the aqueous droplets by using the water-based liquid spring. To precisely control the direction of the droplet motion, on-demand tracks are pre-carved on the superhydrophobic surface, which also has the benefits of reducing the friction between the droplet and the surface. In the direct manipulation of the miscible droplets, there are two outcomes after the actuation. One is that the liquid spring mingles with the target droplet when they contact each other (Video V6, Supporting Information). The other is that the target droplet is flicked away by the liquid spring (Fig. 3a, Video V1, Supporting Information). Prevention of the coalescence between the liquid spring and the target droplet is primarily attributed to the existence of the air cushion between them. Indeed, the air cushion plays an important role in many collision scenarios to separate the miscible droplets[46–48]. The stable existence of the air cushion is dependent on several factors, such as the volume ratio of the target droplet to the liquid spring, the liquid spring deformation velocity, etc. When the volume of the liquid spring is comparable to the target droplet, the air cushion is likely to break up during the collision process and droplets coalescence occurs. Nevertheless, when the liquid spring is much larger than the target droplet, the air cushion is prone to exist during the collision. As a result, the target droplet will be pushed away (Fig. 3a). Detailed parameter analysis is provided in Supporting Information Section 7. For a stable propulsion system, the motion velocity of the target droplet V_t is related with ΔB (Fig. 3b). The correlation is straightforward, as an increase in ΔB results in the transfer of a greater amount of momentum to the target droplet during the collision process. Consequently, the target droplet has a higher V_t. Compared to the passive[1,49–51], light-actuated[24,52–54], electrical[55], and magnetic[36,38,40] methods, the present strategy enables a better trade-off between the volume of the target droplet and its motion velocity (Fig. 3c). It is able to navigate the target droplet ($\approx$ 20 μL) with high motion velocity ($\approx$ 19 cm s^{-1}), which is fourfold higher than other reported magnetic strategies[36,38,39].

The uniform magnetic field, generated by the Helmholtz coil, deforms the ferrofluid droplet with no net force. As a result, the droplet centroid keeps stationary within the coil. The movement of the ferrofluid droplet depends on the non-uniform and asymmetric magnetic field, which exerts non-zero net magnetic force on the liquid spring. The non-uniform and asymmetric magnetic field can be easily generated by the permanent magnet. In this way, the Positioning-Launching routine of the liquid spring is realized with the assistance of an additional permanent magnet and the Helmholtz coil (Fig. 3d, Video V7, Supporting Information). **Positioning**: beneath the substrate, a permanent magnet is positioned, which moves the liquid spring from one spot at a relative distance from the target droplet to a new spot closer to the target droplet. **Launching**: after the positioning routine, the permanent magnet is removed and the external uniform magnetic field generated by the Helmholtz coil is activated to propel the non-magnetic droplet. With this strategy, the utilization of a single liquid spring enables us to manipulate the target droplets across the entire surface of the substrate. This approach offers flexibility in manipulating the target droplets. Additionally, there exist other prototypical methods to control the motion of the non-magnetic droplets (Figs. 3e-g). For instance, when the target droplet and the liquid spring are not aligned with the magnetic field direction, the target droplet can be pushed away at an oblique angle (Fig. 3e, Video V8, Supporting Information). Furthermore, the advance of the target droplet initiated by the actuation can fulfill the on-demand droplets coalescence (Fig. 3f, Video V9, Supporting Information). Besides the manipulation of a single droplet, the motion of collective target droplets is also realized by

depositing multiple non-magnetic droplets near the liquid springs on the substrate (Fig. 3g, Video V10, Supporting Information).

The above strategy is focused on the target droplet in-plane manipulation, which indicates that the non-magnetic droplet moves on the substrate surface. In addition, the liquid spring can be adopted to devise a trampoline on which the manipulation of the non-magnetic droplet out-of-plane is accomplished (Figs. 3h-i). The trampoline is composed of three layers. The top layer is a superhydrophobic flake, on which the target droplet is positioned. The second layer is the ferrofluid droplets, which functions as a 'spring cushion'. Finally, the bottom layer is the substrate foundation for stabilizing the ferrofluid droplets. When the ferrofluid droplets are deposited under both margins of the flake, the target droplet trampolines vertically after the magnetic field is activated because the liquid spring 'stands up' due to the magnetic force (Fig. 3h, Video V11, Supporting Information). When the ferrofluid droplet is placed under the left margin of the flake and the right margin is supported by the non-ferrofluid droplet with the similar size, one end of the flake is levitated and the other stays still after the activation of the magnetic field. The tilting behavior of the flake will cast the target droplet with an oblique velocity (Fig. 3i, Video V12, Supporting Information). With the assistance of the spring trampoline, it is possible for the target droplet on the trampoline to achieve obstacle crossing through out-of-plane motion.

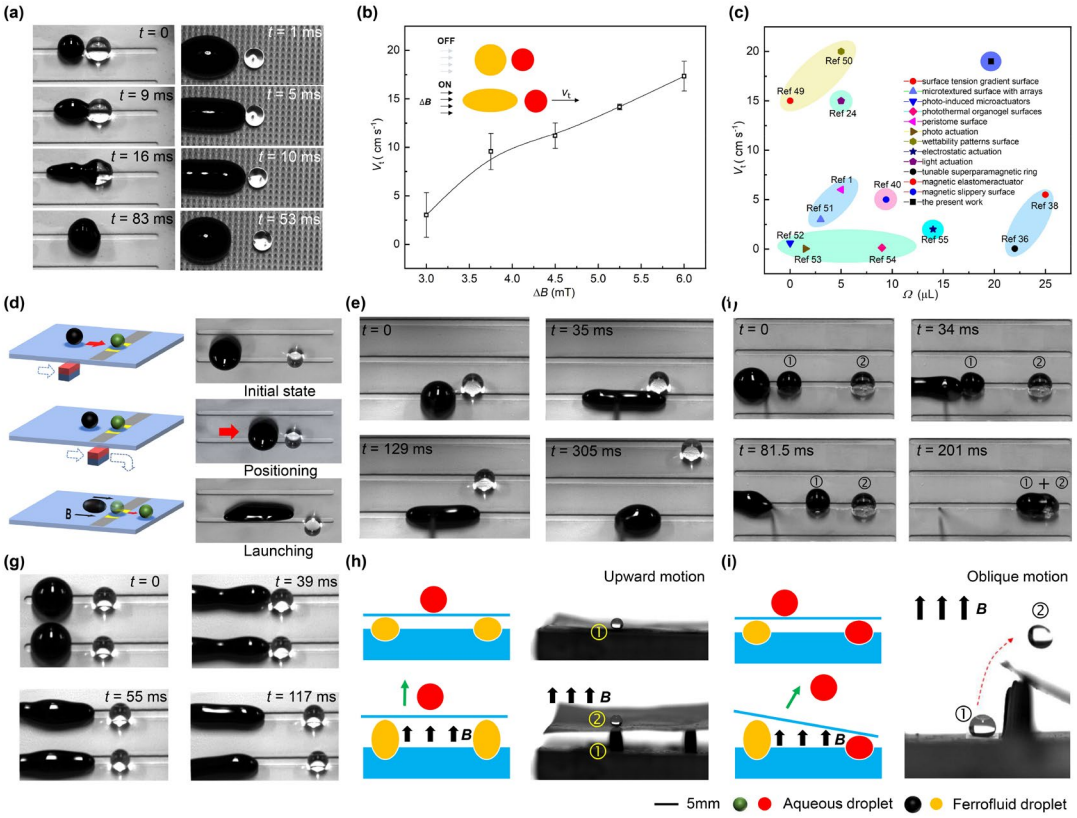

Fig. 3 The water-based liquid springs to manipulate the non-magnetic aqueous droplets. (a) There are two scenarios when the liquid spring collides with the miscible droplet. One is that the liquid spring merges with the miscible droplet when they come into contact with each other. The other is that the liquid spring flicks away the miscible droplet due to the existence of the air cushion between them throughout the collision process. **(b)** The dependence of the target droplet motion velocity V_t on ΔB. The volumes of the spring and the target droplet are 120 μl and 15 μl respectively. It is figured out that V_t increases with ΔB and can reach up to 19 cm s^{-1}. **(c)** Comparison of the present strategy with other reported methods in terms of the target droplet volume Ω and the motion velocity V_t. The present strategy is able to propel a larger target droplet with a higher motion velocity. **(d)**

The Positioning-Launching routine. **Positioning**: the liquid spring at a relatively distant place is migrated to the spot closer to the target droplet by navigating the permanent magnet beneath the substrate. **Launching**: after positioning, the external uniform magnetic field is activated to deform the liquid spring for propelling the non-magnetic droplet. **(e)** Actuating the non-magnetic droplet at an angle to the magnetic field direction. When the liquid spring and the target droplet are not aligned with the magnetic field direction, the actuation results in the target droplet moving at an angle to the magnetic field direction. **(f)** On-demand droplets coalescence. The target droplets are actuated to achieve the on-demand droplets coalescence, in which target droplet 1 is pushed forward to mingle with target droplet 2. **(g)** Propulsion of multiple target droplets. Two liquid springs are placed side by side and the two target droplets will be actuated simultaneously when the magnetic field is activated. **(h)-(i)** Spring trampolining. The ferrofluid droplets, located between the substrate foundation and a superhydrophobic flake, function as a spring trampoline to achieve non-magnetic droplet out-of-plane locomotion. In **(h)**, the ferrofluid droplets locate under both margins of the flake. The non-magnetic droplet will move upwards after actuation. In **(i)**, the ferrofluid droplet only locates under one margin of the flake and the non-ferrofluid droplet of a similar size is deposited under the other margin. When the magnetic field is activated, the asymmetric motion of the flake will eject the target droplet at a tilt angle.

Utilizing the water-based liquid springs to manipulate the water-repellent solid particles

Non-magnetic solid particles are able to be transported through external magnetic field, which is realized by cloaking the particles with a thin layer of ferrofluid[40]. Herein, the liquid spring is demonstrated to possess the similar ability to achieve the movement of the water-repellent solid particles. Unlike propelling a miscible droplet where the liquid spring may mingle with the target droplet, water-repellent solid particles maintain their intrinsic ability to repel the water-based ferrofluid, which makes it much easier to achieve the propulsion of solid particles. The straightforward scheme is to push away the solid particle when the particle and the liquid spring are aligned with the magnetic field direction (Fig. 4a, Video V2, Supporting Information). Upon activation of the magnetic field, the particle is pushed away for a specific distance, determined by ΔB and the mass ratio of the liquid spring to the particle $\widetilde{m_s}$. Fig. 4b illustrates the correlation between the particle motion velocity V_s and ΔB for different $\widetilde{m_s}$. V_s increases with ΔB and larger particles result in lower speed due to the heavier mass.

Furthermore, the liquid spring has the capability to propel the solid particle at an oblique angle when the particle and the liquid spring are not aligned with the magnetic field direction (Fig. 4c, Video V13, Supporting Information). The liquid spring is also capable of manipulating collective solid particles. For instance, two solid particles and a liquid spring are aligned with the magnetic field direction with the liquid spring located between the particles. Upon activation of the magnetic field, the two particles are propelled away and advance in opposite directions (Fig. 4d, Video V14, Supporting Information). When the object sequence is not aligned with the magnetic field direction with one solid particle deviating from the central line, one particle will move forward along the magnetic field direction and the other will advance at an oblique angle after the actuation of the magnetic field (Fig. 4e, Video V15, Supporting Information).

The distinct kinematic responses of particles with different masses to the same actuation can be utilized to achieve mass or density sieving. This is accomplished by depositing two liquid springs of identical size on the solid substrate. One liquid spring is used to propel a larger solid particle, while the other is employed to propel a smaller particle with the same density (Fig. 4f, Video V16, Supporting Information). When the magnetic field is activated, the particles will be ejected at different velocities due to their mass difference. As a result, the heavier particle travels a shorter distance compared to the lighter one. If the two solid particles have similar sizes but different densities, the distance of their movement after actuation can indicate which one has a larger or smaller density. The lighter particle advances a longer distance, while the heavier particle will

remain nearly stationary (Fig. 4g, Video V17, Supporting Information). The liquid spring is also capable of propelling the solid-liquid-solid (SLS) object sequence, which is aligned with the magnetic field direction (Fig. 4h, Video V18, Supporting Information). Initially, the liquid spring impinges on the first water-repellent solid particle, propelling it and actuating the adjacent aqueous droplet. Subsequently, the aqueous droplet pushes away the second water-repellent solid particle, enabling the collective movement of objects with different phases.

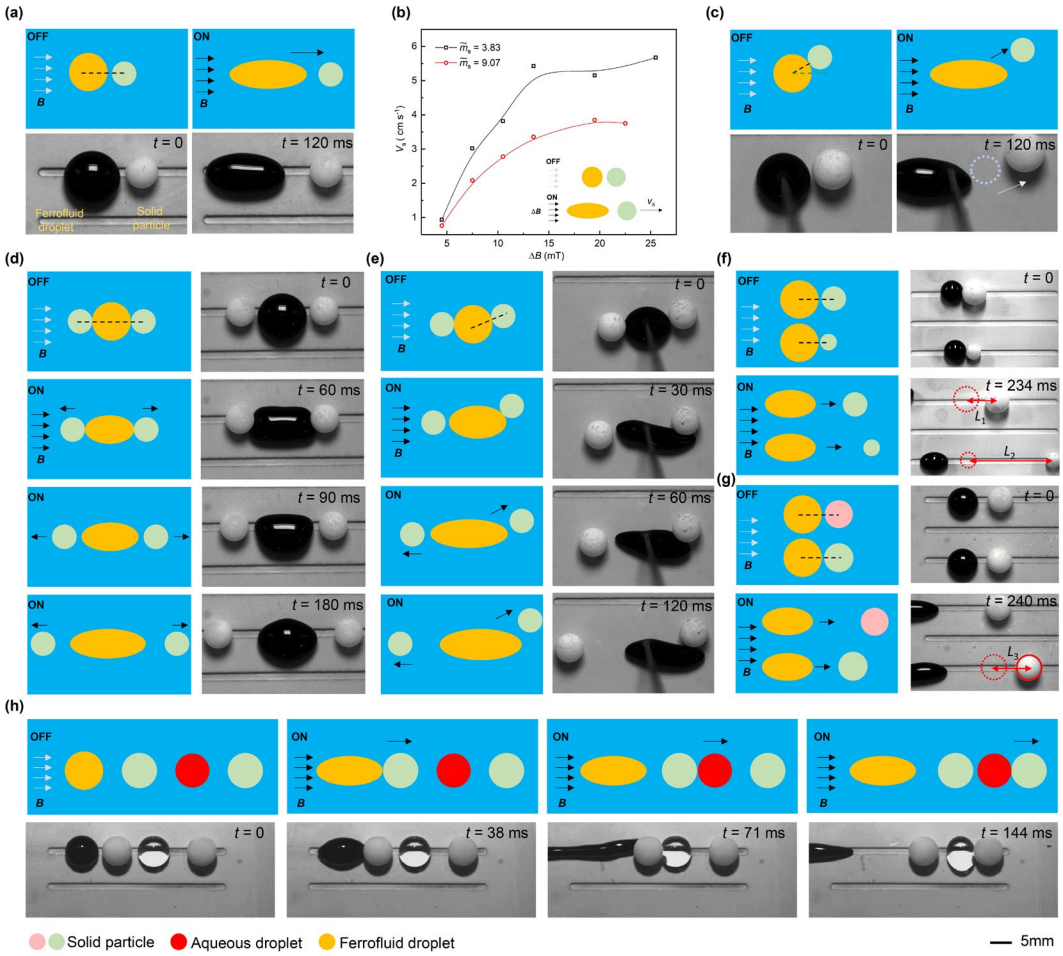

Fig. 4 Utilizing the water-based liquid springs to manipulate the non-magnetic water-repellent solid particles. (a) When the liquid spring and solid particle are aligned with the magnetic field direction, the solid particle will be propelled for a distance after the activation of the magnetic field. **(b)** The dependence of solid particle motion velocity V_s on ΔB and the particle mass for identical spring. It is observed that V_s increases with ΔB and larger particle results in lower speed due to the heavier mass. **(c)** Oblique motion of the solid particle. When the liquid spring and the particle are not aligned with the magnetic field direction, the particle will be propelled at an oblique angle to the magnetic field direction. **(d)-(e)** Actuation of the collective solid particles. **(d)** Two solid particles and a liquid spring line up and are aligned with the magnetic field direction. When the magnetic field is activated, both particles will be propelled along the magnetic field direction. **(e)** Two solid particles and the liquid spring do not line up with one solid particle deviating from the central line. When the magnetic field is activated, two particles will be propelled with one moving along the magnetic field direction and the other advancing at an oblique angle to the magnetic field direction. **(f)-(g)** Mass/density sieving. Two liquid springs of identical size are deposited on the substrate. **(f)** One liquid spring is propelling a larger solid particle (D_s = 5 mm) and the other is propelling a smaller one (D_s = 3 mm). The smaller particle moves further due to the lighter mass. **(g)** One liquid spring is propelling a particle with higher density (5 g cm^{-3}) and the other is propelling a particle with lower density (1.4 g cm^{-3}). When the magnetic field is activated, the two particles will be ejected with different velocities due to the mass difference. The lighter one will advance over a longer distance while the heavier one is almost stationary. L_1, L_2, and L_3 are the moving distances of the solid particles. **(h)** The liquid spring is propelling solid–liquid–solid (SLS) object sequence, enabling the collective movement of objects with different phases.

Discussion

Based on the actuation of a ferrofluid droplet in an external uniform magnetic field, we propose a conceptual liquid spring, which is capable of navigating tiny objects including miscible droplets and solid particles in a contamination-free, efficient, and programmable way. The successful navigation of the miscible droplets is dependent on the stable existence of an air cushion between the liquid spring and the target droplets throughout the collision process, which is influenced by many factors, such as the volume ratio of the liquid spring to the target droplet and the deformation rate of the liquid spring. In the actuation of tiny objects, their motion velocity can be precisely and flexibly adjusted by varying the instant variation value of the magnetic field strength, which is controlled by the electrical current. With the assistance of the liquid spring, some fundamental operations, such as single/multiple droplets/solid particles advancing, the on-demand droplets coalescence, and the droplet out-of-plane motion are achievable. The applications in the present work are conceptual. For the industrial applications, some additional issues, e.g., the large-scale usage, are needed to be considered, which entail future work.

Methods and materials

Fabrication of the superhydrophobic surface: The TiO_2 solution is prepared firstly. 1.00 g of 1*H*, 1*H*, 2*H*, 2*H*-perfluorooctyltriethoxysilane is mingled with 99 g of the absolute ethanol, and the solution is stirred for 2 hours by the magnetic stirrer. After stirring, 6 g of titanium oxide nanoparticles and 6 g of Degussa P25 titanium oxide are added to the solution to make a paint-like suspension. The superhydrophobic surface is prepared by painting the suspension onto the substrate surface, which is then dried for about half an hour. The substrate used in the present study has three types: the micro-structure substrate printed with high-temperature resin, the copper plate with straight routes, and the flake made of hard paper.

Fabrication of the superhydrophobic solid particle: The solid particles are purchased on Taobao. The particle diameter ranges from 2 mm to 5 mm. The materials are of two types: One is polyoxymethylene with a density of 1.4 g cm^{-3} and the other is glass with a density of 5.0 g cm^{-3}. To make the particles superhydrophobic, they are immersed in the TiO_2 solution and taken out for drying for half an hour.

Droplet and particle manipulation experiments: The aqueous droplet is deposited on the non-wetting surface and the contact angle is measured with the equipment (OCA15EC, Dataphysics, Germany) to characterize the wettability of the solid surface. The aqueous droplet motion and the dynamics of the ferrofluid droplets are recorded using the high-speed camera (FASTCAM Nova S9, Japan). The water-based ferrofluid is commercially obtained from Beijing Huayuan Zhenda Magnetic Fluid Technology Co., Ltd. The unidimensional external uniform magnetic field (with the magnetic field strength up to 30 mT), deforming the ferrofluid droplet, is generated by using the Helmholtz coil. The non-uniform magnetic field, navigating the ferrofluid droplet, is generated by the permanent magnet (NdFeB, Grade-N35).

Numerical method: The simulation is performed based on open-source software *Basilisk*, which adopts the finite volume method to discretize the governing equations. The governing equations include mass conservation, momentum conservation, phase equation, and the Maxwell equation.

The phase equation controls the evolution of the liquid-air interface and the Maxwell equation determines the distribution of the magnetic field strength based on magnetic potential scalar. A detailed description of the computational process is included in the supporting information.

Data availability

The data that support the findings of this study are available from the corresponding authors.

Acknowledgements

This work is supported by the Natural Science Foundation of Guangdong Province (Grant No. 2024A1515011811), the Science and Technology Innovation Committee of Shenzhen (Grant No. JSGG20220831101400002), the Guangdong Provincial Key Laboratory of Turbulence Research and Applications (Grant No. 2019B21203001), and the Department of Education of Guangdong Province (Grant No. 2020KZDZX1185). The financial support from the Research Grants Council of Hong Kong (GRF 17213823, 17205421 and 17204420) and the Hong Kong Polytechnic University (SHS Chair Professor P0045687) is also gratefully acknowledged.

Author contributions

H. Z., L. W., and P. Y. conceived the project. H. Z. and Q. D. built the experimental setup. H. Z. and H. D. performed the experiments and interpreted the data. H. Z. and M. G. performed the simulation and analyzed the numerical results. W. L. and Y. Z. provided constructive suggestions in the experimental operation and manuscript writing. L. W. and P. Y. supervised the project.

Competing interests

The authors declare no competing interests.

References

[1] H. Chen, P. Zhang, L. Zhang, H. Liu, Y. Jiang, D. Zhang, Z. Han, L. Jiang, *Nature* **2016**, *532*, 85.

[2] I. S. Farooqi, J. M. Keogh, S. Kamath, S. Jones, W. T. Gibson, R. Trussell, S. A. Jebb, G. Y. H. Lip, S. O'Rahilly, *Nature* **2001**, *414*, 34.

[3] J. Ju, H. Bai, Y. Zheng, T. Zhao, R. Fang, L. Jiang, *Nat. Commun.* **2012**, *3*, 1247.

[4] P. Zhu, L. Wang, *Lab Chip* **2017**, *17*, 34.

[5] G. M. Whitesides, *Nature* **2006**, *442*, 368.

[6] W. Feng, E. Ueda, P. A. Levkin, *Adv. Mater.* **2018**, *30*, 1706111.

[7] X. Tang, P. Zhu, Y. Tian, X. Zhou, T. Kong, L. Wang, *Nat. Commun.* **2017**, *8*, 14831.

[8] M. Jiang, Y. Wang, F. Liu, H. Du, Y. Li, H. Zhang, S. To, S. Wang, C. Pan, J. Yu, D. Quéré, Z. Wang, *Nature* **2022**, *601*, 568.

[9] H. J. Cho, D. J. Preston, Y. Zhu, E. N. Wang, *Nat. Rev. Mater.* **2016**, *2*, 16092.

[10] X. Han, X. Tang, H. Zhao, W. Li, J. Li, L. Wang, *Mater. Horiz.* **2021**, *8*, 3133.

[11] A. Gauthier, S. Symon, C. Clanet, D. Quéré, *Nat. Commun.* **2015**, *6*, 8001.

[12] M. Sharma, S. Gupta, B. Bhatt, G. Bhatt, S. Bhattacharya, K. Khare, *Adv. Mater. Interfaces* **2021**, *8*, 2001916.

[13] J. Hui Guan, É. Ruiz-Gutiérrez, B. B. Xu, D. Wood, G. McHale, R. Ledesma-Aguilar, G. George Wells, *Soft Matter* **2017**, *13*, 3404.

[14] C. Liu, Y. Sun, J. Huanng, Z. Guo, W. Liu, *Adv. Colloid Interface Sci* **2021**, *295*, 102502.
[15] J. Hartmann, M. T. Schür, S. Hardt, *Nat. Commun.* **2022**, *13*, 289.
[16] Y. Jin, W. Xu, H. Zhang, R. Li, J. Sun, S. Yang, M. Liu, H. Mao, Z. Wang, *Proc. Natl. Acad. Sci. U.S.A.* **2022**, *119*, e2105459119.
[17] W. Xu, Y. Jin, W. Li, Y. Song, S. Gao, B. Zhang, L. Wang, M. Cui, X. Yan, Z. Wang, *Sci. Adv.* **2022**.
[18] G. Huang, M. Li, Q. Yang, Y. Li, H. Liu, H. Yang, F. Xu, *ACS Appl. Mater. Interfaces* **2017**, *9*, 1155.
[19] Y. Zhao, J. Fang, H. Wang, X. Wang, T. Lin, *Adv. Mater.* **2010**, *22*, 707.
[20] J. V. I. Timonen, M. Latikka, L. Leibler, R. H. A. Ras, O. Ikkala, *Science* **2013**, *341*, 253.
[21] M. Sun, B. Hao, S. Yang, X. Wang, C. Majidi, L. Zhang, *Nat. Commun.* **2022**, *13*, 7919.
[22] Y. Zhang, Z. Huang, Z. Cai, Y. Ye, Z. Li, F. Qin, J. Xiao, D. Zhang, Q. Guo, Y. Song, J. Yang, *Sci. Adv.* **2021**, *7*, eabi7498.
[23] X. Tang, L. Wang, *ACS Nano* **2018**, *12*, 8994.
[24] W. Li, X. Tang, L. Wang, *Sci. Adv.* **2020**, *6*, eabc1693.
[25] W. Yan, C. Zhao, W. Luo, W. Zhang, X. Li, D. Liu, *ACS Appl. Mater. Interfaces* **2021**, *13*, 23181.
[26] G. Graeber, K. Regulagadda, P. Hodel, C. Küttel, D. Landolf, T. M. Schutzius, D. Poulikakos, *Nat. Commun.* **2021**, *12*, 1727.
[27] J. Li, Y. Hou, Y. Liu, C. Hao, M. Li, M. K. Chaudhury, S. Yao, Z. Wang, *Nat. Phys.* **2016**, *12*, 606.
[28] C. Liu, C. Lu, Z. Yuan, C. Lv, Y. Liu, *Nat. Commun.* **2022**, *13*, 3141.
[29] Y. N. Cheung, N. T. Nguyen, T. N. Wong, *Soft Matter* **2014**, *10*, 8122.
[30] T. Franke, A. R. Abate, D. A. Weitz, A. Wixforth, *Lab Chip* **2009**, *9*, 2625.
[31] H. Zhan, C. Lu, C. Liu, Z. Wang, C. Lv, Y. Liu, *Phys. Rev. Lett.* **2021**, *126*, 234503.
[32] P. Brunet, J. Eggers, R. D. Deegan, *Phys. Rev. Lett.* **2007**, *99*, 144501.
[33] X. Han, W. Li, H. Zhao, J. Li, X. Tang, L. Wang, *Nat. Commun.* **2021**, *12*, 3154.
[34] S. Jiang, Y. Hu, H. Wu, Y. Zhang, Y. Zhang, Y. Wang, Y. Zhang, W. Zhu, J. Li, D. Wu, J. Chu, *Adv. Mater.* **2019**, *31*, 1807507.
[35] Z. Wang, K. Wang, D. Liang, L. Yan, K. Ni, H. Huang, B. Li, Z. Guo, J. Wang, X. Ma, X. Tang, L. Chen, *Adv. Mater.* **2020**, *32*, 2001879.
[36] V. Nasirimarekani, F. Benito-Lopez, L. Basabe-Desmonts, *Adv. Funct. Mater.* **2021**, *31*, 2100178.
[37] A. Li, H. Li, Z. Li, Z. Zhao, K. Li, M. Li, Y. Song, *Sci. Adv.* **2020**, *6*, eaay5808.
[38] K. S. Seo, R. Wi, S. G. Im, D. H. Kim, *Polym. Adv. Technol.* **2013**, *24*, 1075.
[39] J. Zhang, X. Wang, Z. Wang, S. Pan, B. Yi, L. Ai, J. Gao, F. Mugele, X. Yao, *Nat. Commun.* **2021**, *12*, 7136.
[40] U. Banerjee, M. R. Gunjan, S. K. Mitra, *Langmuir* **2024**, *40*, 3105.
[41] X. Zhang, L. Sun, Y. Yu, Y. Zhao, *Adv. Mater.* **2019**, *31*, 1903497.
[42] S. Afkhami, Y. Renardy, M. Renardy, J. S. Riffle, T. St PIERRE, *J. Fluid Mech.* **2008**, *610*, 363.
[43] S. Afkhami, A. J. Tyler, Y. Renardy, M. Renardy, T. G. St. PIERRE, R. C. Woodward, J. S. Riffle, *J. Fluid Mech.* **2010**, *663*, 358.
[44] P. Rowghanian, C. D. Meinhart, O. Campàs, *J. Fluid Mech.* **2016**, *802*, 245.

[45] T. Vieu, C. Walter, *J. Fluid Mech.* **2018**, *840*, 455.
[46] X. Han, X. Tang, H. Zhao, J. Li, W. Li, L. Wang, *Adv. Mater. Interfaces* **2022**, *9*, 2101565.
[47] O. Ramírez-Soto, V. Sanjay, D. Lohse, J. T. Pham, D. Vollmer, *Sci. Adv.* **2020**, *6*, eaba4330.
[48] H. Mertaniemi, R. Forchheimer, O. Ikkala, R. H. A. Ras, *Adv. Mater.* **2012**, *24*, 5738.
[49] S. Daniel, M. K. Chaudhury, J. C. Chen, *Science* **2001**, *291*, 633.
[50] S. Huang, S. Yin, F. Chen, H. Luo, Q. Tang, J. Song, *Appl. Surf. Sci.* **2018**, *428*, 432.
[51] J. Li, Q. H. Qin, A. Shah, R. H. A. Ras, X. Tian, V. Jokinen, *Sci. Adv.* **2016**, *2*, e1600148.
[52] J. Lv, Y. Liu, J. Wei, E. Chen, L. Qin, Y. Yu, *Nature* **2016**, *537*, 179.
[53] D. Baigl, *Lab Chip* **2012**, *12*, 3637.
[54] C. Gao, L. Wang, Y. Lin, J. Li, Y. Liu, X. Li, S. Feng, Y. Zheng, *Adv. Funct. Mater.* **2018**, *28*, 1803072.
[55] H. Dai, C. Gao, J. Sun, C. Li, N. Li, L. Wu, Z. Dong, L. Jiang, *Adv. Mater.* **2019**, *31*, 1905449.